**Steel and Composite Structures**, *Vol. 27*, *No. 1* (*2018*) *123-133*
DOI: https://doi.org/10.12989/scs.2018.27.1.123


# Finite element model for interlayer behavior of double skin steel-concrete-steel sandwich structure with corrugated-strip shear connectors

Mehdi Yousefi [1a] and Mansour Ghalehnovi [*2]

[1] *Civil Engineering Department*, *Faculty of Maritime Engineering*, *Chabahar Maritime University*, *Chabahar*, *Iran*
[2] *Civil Engineering Department*, *Faculty of Engineering*, *Ferdowsi University of Mashhad*, *Mashhad*, *Iran*

(*Received April 22*, *2017*, *Revised September 6*, *2017*, *Accepted February 10*, *2018*)

**Abstract.** Steel-concrete-steel (SCS) sandwich composite structure with corrugated-strip connectors (CSC) has the potential to be used in buildings and offshore structures. In this structure, CSCs are used to bond steel face plates and concrete. To overcome executive problems, in the proposed system by the authors, shear connectors are one end welded as double skin composites. Hence, this system double skin with corrugated-strip connectors (DSCS) is named. In this paper, finite element model (FEM) of push-out test was presented for the basic component of DSCS. ABAQUS/Explicit solver in ABAQUS was used due to the geometrical complexity of the model, especially in the interaction of the shear connectors with concrete. In order that the explicit analysis has a quasi-static behavior with a proper approximation, the kinetic energy (ALLKE) did not exceed 5% to 10% of the internal energy (ALLIE) using mass-scaling. The FE analysis (FEA) was validated against those from the push-out tests in the previous work of the authors published in this journal. By comparing load-slip curves and failure modes, FEMs with suitable analysis speed were consistent with test results.

**Keywords:** steel-concrete-steel sandwich; corrugated-strip connectors; push-out test; explicit analysis; mass-scaling

## 1. Introduction

In recent decades, steel-concrete-steel (SCS) sandwich composite structures composed of two steel face plates and a concrete core have been noticed due to their low cost and resistance. The first application of such these materials was in civil and structural engineering. Their flexibility in weight and thickness and easy-to-make process with popular instruments in construction sites resulted in the development of their application in submerged tube tunnels, floating breakwaters, anti-collision structures, liquid containment, ship hull and offshore deck structures (Wright and Oduyemi 1991). The main advantage of these materials is related to external steel face plates acting as the primary reinforcement and permanent framework and a resistant membrane against leakage, impact and blast. In SCS sandwich structures, cohesive material such as epoxy or mechanical shear connectors are common measures to bond the steel and concrete together. Compared to cohesive material, mechanical shear connectors are more advantageous in terms of transverse shear resistance (Solomon *et al*. 1976). To improve the composite behavior of SCS system, different shear connectors are developed, including C-shaped connectors as in Fig. 1(a) (Shariati *et al*. 2012), L-shaped connectors as in Fig. 1(b) (Soty and Shima 2011), overlapped headed studs in double-skin composite structure (DSC) as in Fig. 1(c) (Tomlinson *et al*. 1989), friction welding connectors in Bi-steel structure as in Fig. 1(d) (Bowerman and Chapman 2000) and J-hook connectors as in Fig. 1(e) (Liew and Sohel 2009, Liew *et al*. 2009, Yan *et al*. 2014, 2015). Valente and Cruz (2010) also studied the performance of light weight concrete in SCS sandwich structures to achieve a light weight concrete and steel composite beam similar to the behavior of composite beam with normal density concrete. There is limited literature on development of corrugated-strip connectors (CSC) (see Fig. 1(f)) that were first proposed by Leekitwattana *et al*. in 2010 (Leekitwattana *et al*. 2010, 2011). One of the advantages of this system compared to other shear connectors is that unlike previous models in which shear connectors are normal to steel face plates, the angle of shear connectors can be aligned perpendicular to diagonal crack line of concrete approximately. In this system, shear connectors are welded to steel face plates from both sides that create thickness limitation in practice and need modern welding equipment to connect both sides of connectors to both steel face plates. Practical restrictions can be the main reason of non-development of these shear connectors.

The idea used in the present article is extracted from DSC and CSC models, since in the proposed system as in Fig. 2, corrugated-strip connectors are used according to CSC model connectors, but like DSC model, connectors are connected to one face and double skin connection is provided by burying shear connectors in the concrete core. The combined system is known as double skin with corrugated-strip connectors (DSCS) system. One of the advantages of the system is that the connector is welded to the plates easily using electric arc welding, and it was

*Corresponding author, Ph.D., Associate Professor,
E-mail: ghalehnovi@um.ac.ir
[a] Ph.D., Assistant Professor, E-mail: m_yousefi@cmu.ac.ir



ISSN: 1229-9367 (Print), 1598-6233 (Online)

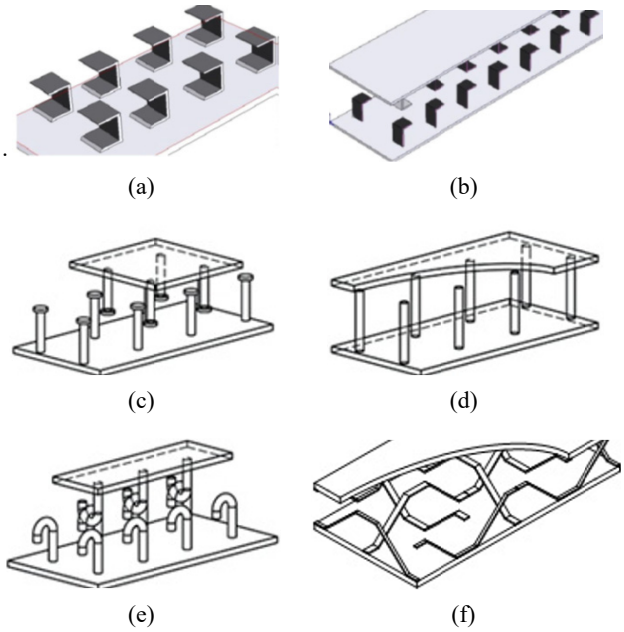


Fig. 1 Shear connectors in SCS sandwich structures. (a) C-shaped connectors; (b) L-shaped connectors; (c) overlapped headed studs in DSC system; (d) friction welding connectors in Bi-steel structure; (e) J-hook connectors; (f) corrugated-strip connectors (CSC)

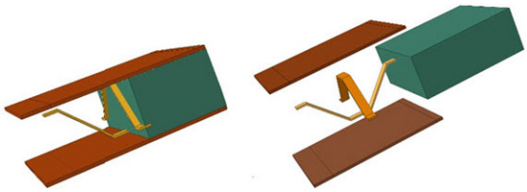

Fig. 2 The proposed SCS sandwich structure

expected that the connection between connectors and steel face plate is supplied according to the adequate weld line. Also it was necessary that the system can provide a suitable interlayer slip control against the loads applied. Hence Yousefi and Ghalehnovi (2017) investigated interlayer behavior of DSCSs under push-out test. Although one end welded CSCs could not be as well as two end welded ones, executive problems were minimized. In any case, a more detailed examination would require costly experiments. Therefore, a numerical model must be presented.

Among analytical methods, numerical methods are useful tools, especially Finite Element Method (FE). Although there is no information on Finite Element Analysis (FEA) of CSCs, there are a few works on other forms of SCS sandwich structure in literature. A simplified model is developed for double skin structure with overlapped headed studs (DSC) (Shanmugam *et al*. 2002). In this model, the concrete core is simplified into a homogeneous non-isotropic material by increasing the shear strength due to shear connectors without modeling shear connectors. This simplification decreases the problem of overlapped connectors modeling in concrete core and total values of elements significantly. Nonlinear spring elements are also used in FE model to replace headed stud connectors and to connect concrete slab to I-shaped steel profile in steel-concrete composite structure (Smitha and Kumar 2013). Zou *et al*. (2016) presented a model similar to this numerical model in which the failure mechanism of steel-concrete-steel beams are examined only based on the interaction of steel face plates and concrete and without modeling shear connectors. However, these simplifications could not reflect the structural behavior of shear connectors and the interaction between shear connectors and concrete, and they chose the transverse shear resistance of the structure less than the actual value. A two-dimensional FE model is also developed for Bi-steel beams (Foundoukos and Chapman 2008). The two-dimensional FE model limits the simulation of the interaction between shear connector and concrete that is usually three-dimensional and significantly affects the shear strength of connectors. In SCS sandwich structure with J-hook connectors, coupling and locking connectors together result in the transfer of longitudinal shear force, resistance against transverse shear and prevention from local buckling of steel face plates. Due to their important role in sandwich structures, their structural behavior must be included in FEA. The complex geometry of J-hook connectors also created challenges for FEA of SCS sandwich beams. To overcome the model complexity, hooks of connectors were eliminated in modeling and instead, nonlinear spring element was used to model the connection between two connectors where the hooks are interlocked (Yan 2015, Huang and Liew 2016).

In any case, none of these methods can be used for CSCs due to the complicated interaction between connectors and concrete. For this reason, ABAQUS/Explicit quasi-static solver is used in the present study by creating finite element model with minimal simplification in geometric shape (ABAQUS and Manual 2010). For this purpose, 12 push-out tests with different geometrical parameters are simulated. Mass-scaling is used to save the time of the analysis of numerical models. In order that the explicit analysis has a quasi-static behavior with a proper approximation, the kinetic energy (ALLKE) did not exceed 5 to 10% of the internal energy (ALLIE) using mass-scaling. Finally, The FEA was validated against those from the push-out tests in the previous work of the authors (Yousefi and Ghalehnovi 2017).

## 2. Push-out test

CSC connectors in SCS sandwich structures play an important role in transferring longitudinal shear force in the interface between steel and concrete, supplying transverse shear force through creating shear cracks connection in concrete and preventing from local buckling and rise of steel face plates (see Fig. 3). Therefore, finite element model must cover these structural behaviors properly. One of the most important features of structural behavior is longitudinal shear behavior that is studied in the present research. Generally, push-out test is employed to obtain ultimate shear strength and load-slip behavior of connectors (Xie *et al*. 2005).

In this study, 12 push-out tests performed by the authors

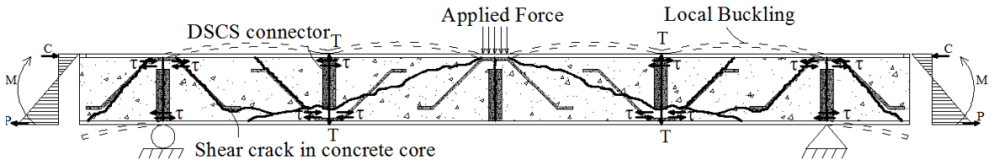


T: Tension force of connector; C: Compressive forces in the section;
P: Tensile forces in the section; M: Bending moment; $\tau$: Interfacial shear force in the connector

Fig. 3 Transfer of internal forces and supply of transverse shear resistance by CSC connectors

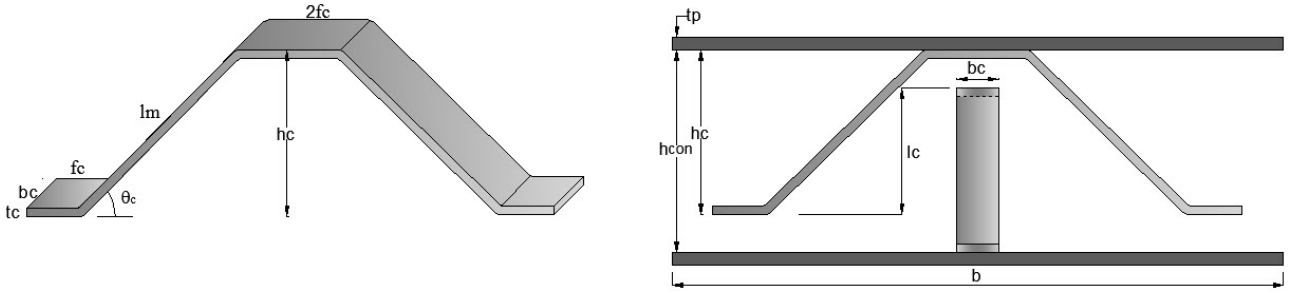


Fig. 4 Naming geometrical dimensions of test samples and CSC connectors (Yousefi and Ghalehnovi 2017)

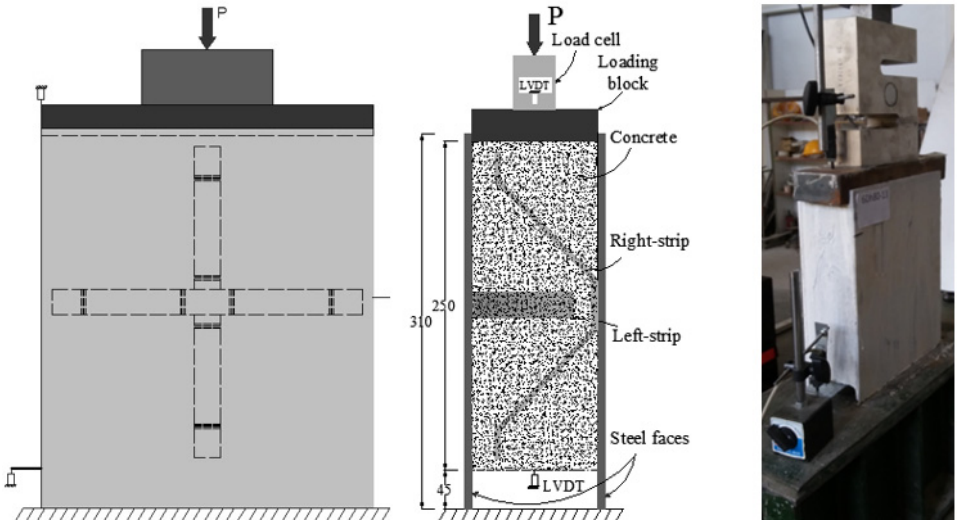


Fig. 5 Test setting (Yousefi and Ghalehnovi 2017)

(Yousefi and Ghalehnovi 2017) are used to verify FE model. Geometrical dimensions of samples and CSC connectors are named in Fig. 4 and their dimensions are listed in Table 1. In Fig. 5, push-out test setting is shown. According to Fig. 5, quasi-static load is applied to the rigid component through load cell and then, it is transferred to the concrete core and CSC connectors. LVDTs are used to register the slip between concrete and steel face plates. Finally, shear force against the slip of any sample is registered by data processing system.

## 3. Finite element model

ABAQUS CAE Software and explicit Solver are used to make the finite element model of push-out tests under quasi-static loading.

### *3.1 Explicit quasi-static analysis*

Dynamic explicit solution is usually used to solve two groups of mechanical processes including quasi-static analysis and transient dynamic response. Quasi-static analysis is used for processes including complex nonlinear effects such as complex conditions of contact. Explicit integration uses very small time steps and central difference operator can be stable or unstable in terms of temporal conditions. Stability limit estimation is automatic in ABAQUS/Explicit software and there is no need for user's intervention. The real value of the biggest frequency in the system is based on some complex factors that are related to each other and the precise value cannot be obtained. So, an effective conservative estimate is used in this software. In other words, maximum frequency is calculated for any element of model instead of considering the whole model.

Table 1 Geometrical dimensions of DSCS samples for push-out test (Yousefi and Ghalehnovi 2017)

| Unit | mm | | | | | | ° | Dimensionless | | |
|---|---|---|---|---|---|---|---|---|---|---|
| | Face plates thickness | Connector width | Flat leg length | Connector height | Connectors overlapped length | Concrete thickness | Connectors sides angle | | | |
| Specimen | $t_p$ | $b_c$ | $f_c$ | $h_c$ | $l_c$ | $h_{con}$ | $\theta_c$ | $hh = h_c/h_{con}$ | $lhl = l_c/h_{con}$ | $k_{cb} = b_c/b$ |
| 6D-1 | 6 | 20 | 27.90 | 79 | 56 | 100 | 45 | 0.79 | 0.56 | 0.08 |
| 8D-2 | 8 | 20 | 27.90 | 79 | 56 | 100 | 45 | 0.79 | 0.56 | 0.08 |
| 10D-3 | 10 | 20 | 27.90 | 79 | 56 | 100 | 45 | 0.79 | 0.56 | 0.08 |
| 12D- 4 | 12 | 20 | 27.90 | 79 | 56 | 100 | 45 | 0.79 | 0.56 | 0.08 |
| 6Db70-5 | 6 | 70 | 27.90 | 79 | 56 | 100 | 45 | 0.79 | 0.56 | 0.28 |
| 6Da90- 6 | 6 | 20 | 25.50 | 79 | 56 | 100 | 90 | 0.79 | 0.56 | 0.08 |
| 6Da60-7 | 6 | 20 | 27.40 | 79 | 56 | 100 | 60 | 0.79 | 0.56 | 0.08 |
| 6Dh100w-8 | 6 | 20 | 26.20 | 100 | 100 | 100 | 55 | 1.00 | 1.00 | 0.08 |
| 6Dh100- 9 | 6 | 20 | 26.20 | 100 | 100 | 100 | 55 | 1.00 | 1.00 | 0.08 |
| 6Dh80- 10 | 6 | 20 | 25.20 | 79 | 73 | 85 | 53 | 0.93 | 0.86 | 0.08 |
| 6Dh65- 11 | 6 | 20 | 25.00 | 64 | 58 | 70 | 53 | 0.91 | 0.83 | 0.08 |
| 6Dh55- 12 | 6 | 20 | 26.00 | 54 | 48 | 60 | 55 | 0.90 | 0.80 | 0.08 |

*Notes: width of steel face plates $b$ = 250 mm, thickness of corrugated-strips $t_c$ = 4 mm

According to this element-to-element method, for any time step, the basic value $\Delta t$ can be calculated in terms of the element's characteristic length obtained in the previous step ($L_e$) and also the current wave velocity ($c_d$) inside the material as follows (ABAQUS and Manual 2010)

$$\Delta t_{stable} = \frac{L_e}{c_d} \tag{1}$$

Wave velocity is also a characteristic of the material that is calculated as Eq. (2) and is calculated by Eq. (3) for elastic material with zero poisson's ratio in the software (ABAQUS and Manual 2010)

$$c_d = \sqrt{\frac{\lambda + 2\mu}{\rho}} \tag{2}$$

$$c_d = \sqrt{\frac{E}{\rho}} \tag{3}$$

Where $\lambda$ and $\mu$ are Lame constants, $E$ is Young's modulus and $\rho$ is density of material. According to Eq. (2), it is clear that the increase in density can decrease the wave velocity, and stable time step increases according to Eq. (1). Using the same principle, explicit solver presents a technique to decrease the time of simulation that is known as mass-scaling. In this technique, the total mass of the model or a part of it increases virtually and the stable time step also increases. If mass-scaling is performed correctly, it can keep the solution precision at an acceptable level in addition to decreasing the solution time. An important point is that mass-scaling techniques used in quasi-static problems can be completely different for transient dynamic problems. Mass-scaling can be performed in ABAQUS/ Explicit in several ways (ABAQUS and Manual 2010):

(1) Mass-scaling of all elements with a constant that is given by the user to the software.
(2) Indirect mass-scaling in which the user uses an arbitrary time step for the whole model instead of determining the mass index for elements. In this case, minimum stable time step of all elements is equal to the limit defined by the user.
(3) Indirect mass-scaling in which the user requires the software to use the time step defined by him only for elements whose stable time step is less than the limit.
(4) Automatic mass-scaling that is determined by the software based on the mesh geometry used and initial conditions.

In the present study, loading time is increased until the acceleration vanishes. The increase in loading time significantly increases the analysis time. Therefore in the next step, the second way of mass-scaling is used that is based on an arbitrary time step for the whole model in order that the analysis time is reduced. Loading time and time step must be chosen in a way that the model is affected by quasi-static loading.

### 3.2 Verification of results

A suitable method for controlling problem solution using quasi-static technique is to compare kinetic and internal energies. A quasi-static solution is acceptable when the kinetic energy does not exceed 5% to 10% of the internal energy. The lower the kinetic energy is, the higher

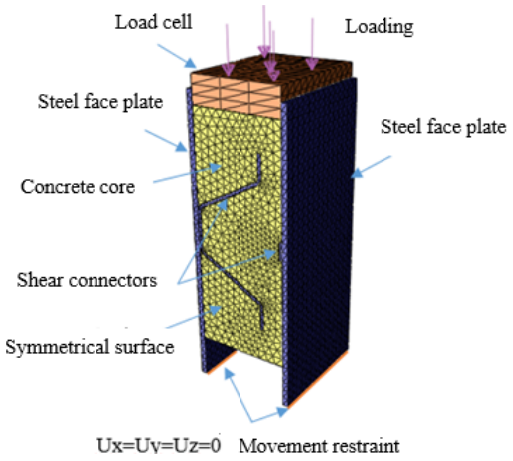


Fig. 6 Finite element model for push-out test

the solution precision will be. Of course, it must be noted that the ratio of kinetic energy to internal energy is not enough to verify problem solution. In addition, two energies must be evaluated logically and independently. Even if the kinetic energy is low but it has many fluctuations, the model has significant plasticity. If loading is applied moderately but the output energy fluctuates, the results of the analysis are not acceptable. Using explicit solver for quasi-static analysis needs a suitable loading rate.

## 4. FE model for push-out test

According to Fig. 6, components of push-out test including steel face plates, shear connectors, concrete core and load cell are modeled by 3D four-node linear tetrahedron (C3D4). This type of mesh is chosen due to the complexity of the contact region of shear connectors and concrete core. For a pair of CSC connector, only a half of sample is made in FE model by taking structural symmetry and loading into account. The overall mesh sizes as 9, 10, 12, 15 and 20 mm are investigated. According to Fig. 6, finer mesh size is used for a better simulation in the bond between shear connectors and steel face plates and positions of contact between connector and concrete core. Four parallel cores of CPU have been used to analyze the models.

### *4.1 Concrete and steel modeling*

Two basic materials are introduced into FE analysis, i.e., steel and concrete.

#### *4.1.1 Concrete modeling*

Concrete damage plasticity (CDP) model was used for concrete core material in push-out test simulation. The CDP model uses the concept of isotropic damaged elasticity in combination with isotropic tensile and compressive plasticity to represent the inelastic behavior of concrete. In contrast to the Brittle Cracking Model it allows the definition of strain hardening in compression and can be defined to be sensitive to the straining rate, which resembles the behavior of concrete more realistically. The model is based on continuous plastic behavior in which two main failure mechanisms are taken into account including compressive crushing and tension crack of concrete. The yield function proposed by Lubliner *et al*. (1989) and modified by Lee and Fenves (1998) is used for a different evaluation of the strength under the effect of tension and compression. In this model, isotropic damage and independent potential current law are assumed (ABAQUS and Manual 2010). Compressive and tensile responses of concrete through CDP are shown in Fig. 7.

According to Fig. 7, it is observed that load-carrying response of the concrete sample has declined due to damage or decrease in elastic stiffness of material. The decrease in elastic stiffness is determined on the softening branch of stress-strain curve using two damage variables $d_t$ and $d_c$ that range from 0 to 1. The zero value shows that the material is not damaged and the value one shows the general decline of strength. The value of the parameters is a function of geometry and type of reinforced concrete model. These parameters are determined through trial and error and comparison with test results or other reliable analyses in different structures (ABAQUS and Manual 2010). In the curves in Figs. 7(a)-(b), $E_0$ is the elastic stiffness of undamaged material and $\tilde{\varepsilon}_t^{pl}, \tilde{\varepsilon}_c^{pl}, \tilde{\varepsilon}_t^{ck}, \tilde{\varepsilon}_c^{in}$ are tensile plastic strain, compressive plastic strain, tensile cracking strain and compressive inelastic strain, respectively. The stress-strain relations under the effect of uniaxial compression and tension are as follows

$$\sigma_t = (1 - d_t).E_0.(\varepsilon_t - \tilde{\varepsilon}_t^{pl}) \quad (4)$$

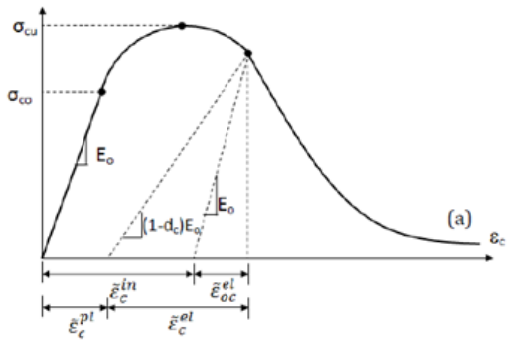


(a) Compressive stress-strain model

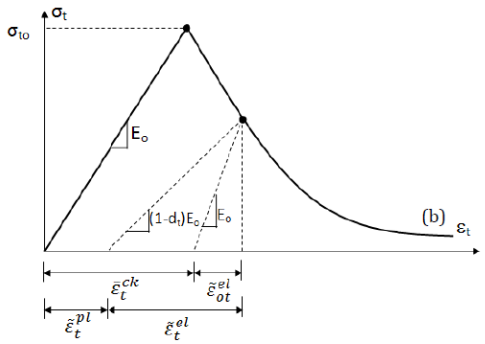


(b) Tension stress-strain model

Fig. 7 Stress-strain model of concrete (Lee and Fenves 1998)

Table 2 Tensile stress-strain values of the concrete 37 MPa and tension damage index

| Stress ($\sigma_t$) (N/mm$^2$) | Cracking strain ($\tilde{\varepsilon}_t^{ck}$) | Damage ($d_t$) |
|---|---|---|
| 3.2 | 0 | 0 |
| 0.032 | 0.00111 | 0.9 |

Table 3 Compressive stress-strain values of the concrete 37 MPa and compression damage index

| Stress ($\sigma_t$) N/mm$^2$ | Inelastic strain ($\tilde{\varepsilon}_c^{in}$) | Damage ($d_t$) |
|---|---|---|
| 16.0 | 0 | 0.0 |
| 21.5 | 0.00013 | 0.0 |
| 23.5 | 0.00015 | 0.0 |
| 33.2 | 0.00038 | 0.0 |
| 37.0 | 0.00077 | 0.1 |
| 25.0 | 0.00204 | 0.3 |
| 14.1 | 0.00340 | 0.5 |
| 5.1 | 0.00597 | 0.7 |
| 2.3 | 0.00794 | 0.9 |

Table 4 Plastic behavior parameters of concrete

| $\psi$ | Eccentricity | $f$ | $k$ | Viscosity parameter |
|---|---|---|---|---|
| 38 | 0.1 | 1.16 | 0.667 | 0.001 |

$$\sigma_c = (1 - d_c).E_0.(\varepsilon_c - \tilde{\varepsilon}_c^{pl}) \quad (5)$$

Also, cracking strain, $\tilde{\varepsilon}_t^{ck}$, and compressive inelastic strain, $\tilde{\varepsilon}_c^{in}$, can be obtained as follows

$$\tilde{\varepsilon}_t^{ck} = \varepsilon_t - \varepsilon_{ot}^{el} \quad (6)$$

$$\tilde{\varepsilon}_c^{in} = \varepsilon_c - \varepsilon_{oc}^{el} \quad (7)$$

Here, $\varepsilon_{ot}^{el} = \sigma_t / E_0$ and $\varepsilon_{oc}^{el} = \sigma_c / E_0$ that are tensile and compressive elastic strains for undamaged material, respectively. Tensile stress-strain values and their tension damage index are listed in Table 2 and compressive stress-strain values and their compression damage index are listed in Table 3.

Other parameters of plastic behavior of concrete include dilation angle, $\psi$, plastic flow potential eccentricity, characteristic parameter of failure function, i.e., the ratio of biaxial to uniaxial compressive strain, $f = f_{b0} / f_{c0}$, parameter of distortion of stress plane or confinement angle, $k$, and viscoplastic parameter for plastic damaged model based on ABAQUS Manual as in Table 4.

#### 4.1.2 Steel modeling

Isotropic/kinematic stiffening model with Von Mises yield criterion is used to define yielding for steel material in ABAQUS Material Library. Elastic Young's modulus, $E_s$, and poisson's ratio must be defined for elastic behavior of steel material. Plastic behavior is defined for steel thickness

Table 5 The mechanical properties of steel

| Thickness (mm) | 0.2% proof stress MPa) | Ult. Stress (MPa) | $\varepsilon_s$ in Ult. Stress | $E_s$ (GPa) |
|---|---|---|---|---|
| 4 (CSCs) | 250 | 380 | 0.3 | 207 |
| 6 | 285 | 495 | 0.23 | 202 |
| 8 | 411 | 615 | 0.176 | 205 |
| 10 | 367 | 620 | 0.198 | 203 |
| 12 | 310 | 516 | 0.180 | 207 |

4, 6, 8, 10 and 12 mm based on stress-strain curve obtained from direct tensile test of dog-bone shaped samples. Properties of steel materials with their thicknesses are obtained based on the test and are summarized in Table 5.

### 4.2 Boundary conditions, loading, interactions and solutions

In push-out test modeling, the lower end of steel face plates is bound against displacement in all directions as in Fig. 6. In the Fig. 6, it is observed that bounds of rotation around Y and Z axes and displacements in X-axis are applied to the symmetry surface. According to Fig. 6, quasi-static loading is applied to the rigid component. The contact between concrete and steel face plates and the contact between connectors and concrete core are surface-to-surface simulated with hard contact formulation in normal direction and penalty friction in tangential direction. In the Interaction Menu of ABAQUS Library, hard formulation means that when two surfaces are contacted, pressure is transferred; however, when they are separated, no force is transferred. Penalty friction means that there is a relative slip between two contact surfaces and the interacting friction force is proportional to the defined friction coefficient. This contact makes it possible that two contact surfaces are separated but they cannot penetrate into each other. Friction coefficient is taken as 0.2 for CSCs and steel face plates that interact with concrete. This value is taken as zero for concrete loading surface and rigid block interaction. The connection between connector and steel face plates is full-bound, and since there is no failure in the welding area almost in all samples, welded connection modeling is ignored.

Mass-scaling is used in explicit solver for quasi-static analysis. Many control parameters are related to convergence criterion in ABAQUS/Explicit. Normally, there are predefined values that are set in a way that the precision and effectiveness of solution are optimized for a wide range of nonlinear problems.

### 4.3 Quasi-static behavior of finite element model

In the tests performed, loading rate is similar to static behavior and can be independent of acceleration. For this reason, finite element models must also show quasi-static behavior. As it was mentioned in previous sections, kinetic and internal energies can be suitable criteria for evaluation of the analysis results. For this purpose, kinetic energy curve must not have excessive fluctuations and must not

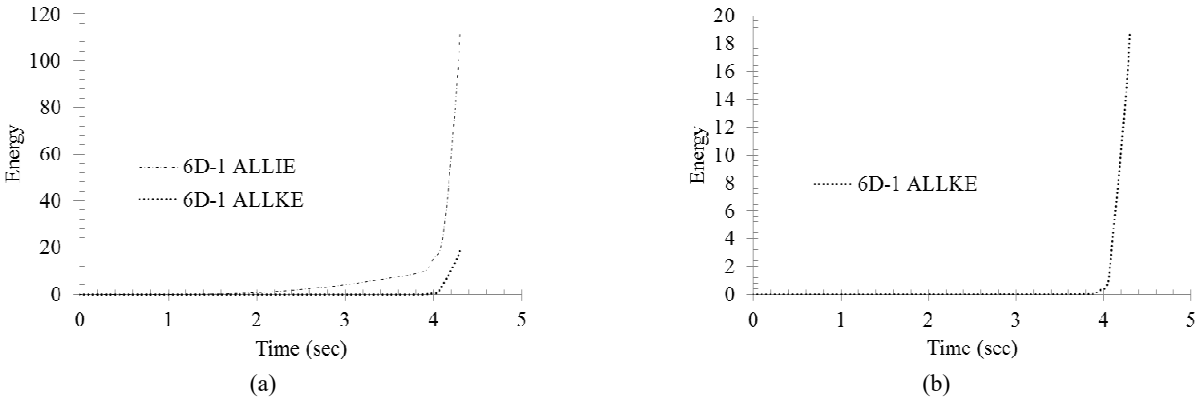


Fig. 8 (a) Comparison between kinetic energy and internal energy of finite element model for the sample 6D-1; (b) kinetic energy of FE model of the sample 6D-1

Table 6 Comparison between kinetic energy and internal energy of modeling of different test samples

| Name | Total time | Ult. strength time | CPU time (sec) | Target time incre. | *ALLIE* | *ALLKE* | $\frac{ALLKE}{ALLIE}$ |
|---|---|---|---|---|---|---|---|
| 6D-1 | 5 | 4.05 | 857 | 0.0001 | 17.5 | 1.011 | 0.058 |
| 8D-2 | 5 | 3.95 | 388 | 0.0003 | 11.37 | 1.05 | 0.092 |
| 10D-3 | 5 | 4.00 | 402 | 0.0003 | 10.95 | 0.99 | 0.091 |
| 12D-4 | 5 | 4.02 | 400 | 0.0003 | 10.78 | 0.99 | 0.092 |
| 6Db70-5 | 5 | 3.82 | 824 | 0.0003 | 82.86 | 8.88 | 0.10 |
| 6Da90-6 | 5 | 3.45 | 1134 | 0.0002 | 66 | 7.25 | 0.10 |
| 6Da60-7 | 5 | 3.77 | 927 | 0.0002 | 51.65 | 5.48 | 0.10 |
| 6Dh100w-8 | 1 | 0.76 | 812 | 0.00005 | 521 | 54.6 | 0.10 |
| 6Dh100-9 | 1 | 0.64 | 12454 | 0.000005 | 306 | 31.2 | 0.10 |
| 6Dh80-10 | 1 | 0.70 | 14008 | 0.000005 | 114.00 | 1.78 | 0.035 |
| 6Dh65-11 | 5 | 3.85 | 1175 | 0.0002 | 33.91 | 3.59 | 0.10 |
| 6Dh55-12 | 5 | 4.17 | 1173 | 0.0002 | 101.2 | 10.59 | 0.10 |

exceed 5% to 10% of the internal energy. To achieve this purpose, loading time must increase as much as possible and a suitable time step must be used. Fig. 8(a) shows that the kinetic energy of finite element model of 6D-1 sample is in an acceptable range compared to its internal energy before failure; however, the kinetic energy suddenly increased in case of failure. Evidently, kinetic energy significantly increases with failure of concrete and plastic behavior of connectors. Fig. 8(b) also shows that kinetic energy does not have many fluctuations and shows a logical behavior. Generally, Fig. 8 shows that in 6D-1 sample, quasi-static behavior is modeled correctly.

In Table 6, kinetic and internal energies of other samples are compared for ultimate strength. Table 6 shows that kinetic energy did not exceed 5% to 10% of the internal energy. This issue makes explicit modeling close to quasi-static behavior desirably. Using target time step is one of the mass-scaling methods. The only difference is that time step is changed instead of increasing density of material. The effect of the change in time step is examined in table 6. Table 6 shows that in the samples 6D-1, 8D-2, 10D-3 and 12D-4 with similar meshing, the analysis time halved as the time step increased from 0.0001 to 0.0003 and it has decreased from 857 s to 400 s. Also in samples 6Dh100w-8 and 6Dh100-9 with similar meshing, as time step increased from 0.000005 to 0.00005, the analysis time decreased about 84%. Using the time step 0.0002 in samples 6Dh65-11 and 6Dh55-11 that have similar meshing as the thickness of concrete slightly decreases, the analysis time is almost the same. Anyway, unsuitable time step can lead to instability before the analysis finishes. For the samples 6Dh100w-8, 6Dh100-9 and 6Dh80-10, a suitable relation is obtained between the kinetic energy and internal energy with overall loading time 1 s. However in other samples, the overall loading time increased to 5 s to provide a suitable relation between kinetic and internal energies.

### *4.4 Verification of finite element model based on test results*

In this section, FEA verification is performed based on load-slip curves of DSCS connectors, ultimate shear strength and failure modes resulting from push-out test.

#### *4.4.1 Load-slip curves of push-out test*

Load-slip curves of FEA are compared with test results

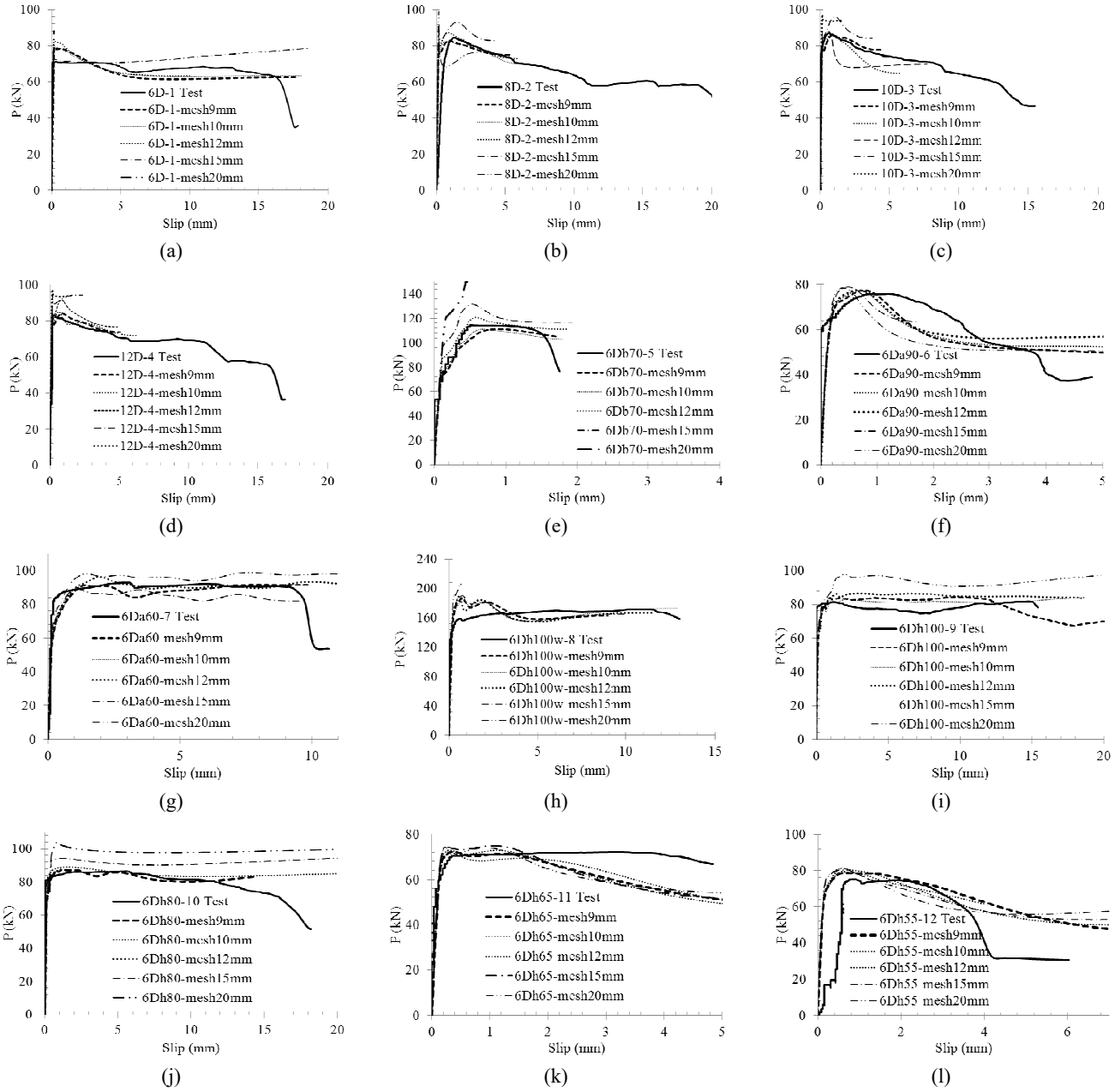


Fig. 9 Comparison of load-slip curve between tests and finite element model

for 12 test samples and finite element model in Figs. 9(a)-(l). To investigate the effect of mesh size on model behavior, all samples with a mesh size of 9, 10, 12, 15, and 20 mm were modeled. The mesh size of 9 mm had the lowest number of distorted elements in the interaction region of the shear connectors and concrete core. Also, according to Fig. 9, it is best to match the test results. By increasing the mesh size from 9 mm to 10 mm and 12 mm, no significant change is observed in the graphs, but with increasing mesh size to 15 and 20 mm in most samples there is considerable discrepancy due to a significant increase in distorted elements. The figures show that the load-slip curves obtained from FEA are consistent with test curves in terms of initial elastic stiffness, threshold of plastic behavior and nonlinear load-slip behaviors. In some specimens e.g., load-slip curves of 6Da90-6 and 6Dh65-11, there is a mismatch in the nonlinear part. This mismatch can be due to the splitting of concrete that cannot well be simulated in the FE model. One of the main reasons of error in comparison of curves can be also related to the kinetic energy that affects the analysis results with its sudden increase in the threshold of plastic behavior. The second reason can be simplification of concrete behavior model as a homogeneous isotropic material that can affect the numerical model and change the test conditions, especially in plastic behavior region. Also, simplification of welded connection and using full connection in finite element model can affect the results of numerical analysis, even though slightly.

#### *4.4.2 Ultimate shear strength and failure modes of push-out test*

Table 7 Comparison of test results and finite element model

| Test ref. | $P_{Test}$ (kN) | Test failure mode | $P_{FE}$ (kN) | FE failure mode | $\frac{P_{Test}}{P_{FE}}$ |
|---|---|---|---|---|---|
| 6D-1 | 71.16 | SS | 78.5 | CC | 0.91 |
| 8D-2 | 84.51 | SS | 82.9 | SS | 1.02 |
| 10D-3 | 86.7 | CC | 85.8 | CC | 1.01 |
| 12D- 4 | 82.95 | SS | 84.2 | CC | 0.99 |
| 6Db70-5 | 114.53 | CC | 110.9 | CC | 1.03 |
| 6Da90- 6 | 75.71 | SS | 77.5 | SS | 0.98 |
| 6Da60-7 | 92.82 | SS | 91.7 | SS | 1.01 |
| 6Dh100w-8 | 171.75 | CC | 186.8 | CC | 0.92 |
| 6Dh100- 9 | 81.36 | SS | 84.6 | SS | 0.96 |
| 6Dh80- 10 | 86.05 | SS | 87.2 | SS | 0.99 |
| 6Dh65- 11 | 72.13 | CC | 72.4 | CC | 1.00 |
| 6Dh55- 12 | 75.33 | CC | 78.7 | CC | 0.96 |
| **Mean** | | | | | **0.98** |
| **Cov.** | | | | | **0.038** |

*Notes: CC concrete cracking failure; SS shear shank failure

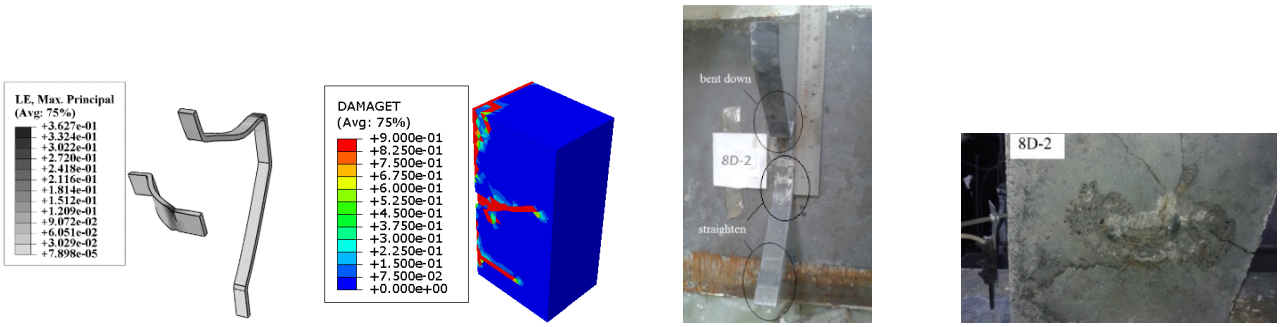


(a) Concrete cracking as herringbone around the bond of connectors and steel face plates

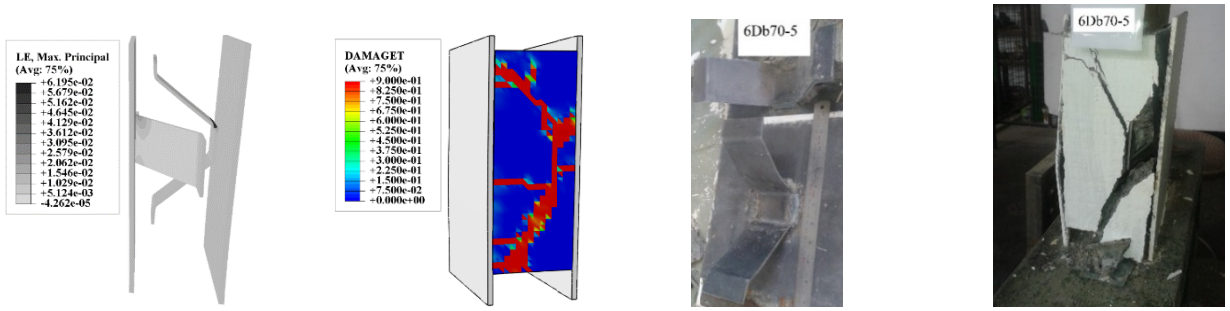


(b) Crack development along the vertical branch of connectors

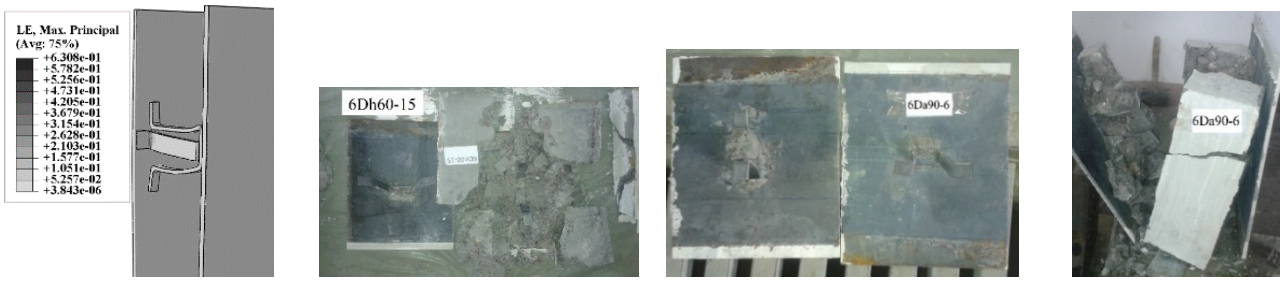


(c) Concrete crushing

Fig. 10 Comparison of failure modes between the test and finite element model

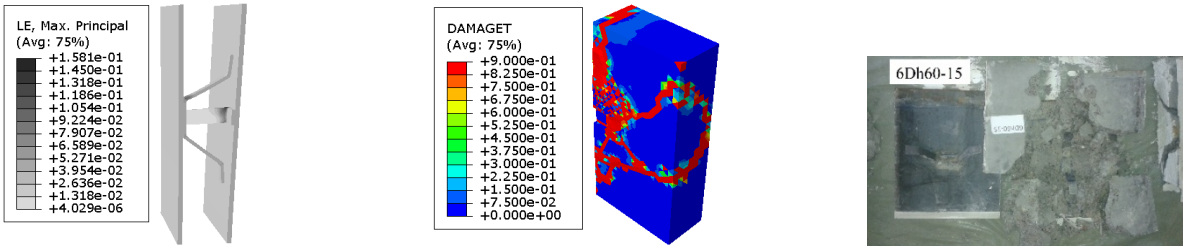


(d) Concrete crushing

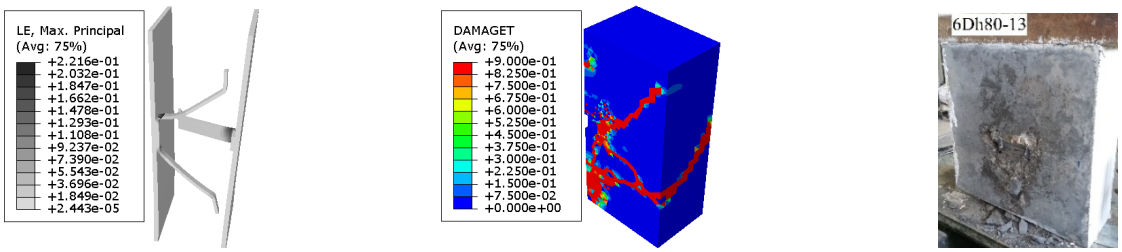


(e) Shear shank failure as test and concrete crushing as FEA

Fig. 10 Continued

Ultimate shear strength of CSC connectors from FEA are compared with shear strengths of push-out tests in table 7. According to the table, the mean ratio of ultimate shear strength test to its prediction is 0.98 for 12 push-out tests with a Coefficient of Variance (COV) 0.038. It can be concluded that ultimate shear strengths of CSC connectors obtained from FEA are consistent with test results.

Two types of failure modes observed in push-out test are shear shank failure (SS) and concrete cracking failure (CC). Fig. 10 shows the comparison of CC and SS failure modes in the test and finite element model. The main contours of plastic strain are used in finite element model to help the judgment on these two types of material. Tension damage index, $d_t$, is defined to show the tension crack growth in concrete. Also, plastic strain is limited to 0.3 (see Table 5) to limit the tension crack of CSC connectors. If strains exceed the permitted value in steel members, failure of steel sections is expected. According to Fig. 10, it is observed that these failure modes can be simulated by finite element model well. According to Fig. 10(a), failure mode of connector occurred for the sample 8D-2 in the test in a way that tension crack of concrete was developing as herringbone around the bond of connectors and steel face plates. Finite element model also shows that the trend of cracks development in the model was consistent with the test and plastic strain at the end of connectors did not exceed 0.3. According to Fig. 10(b) in 6Db70-5 sample, the test and modeling show that the increase in the breadth of connector resulted in the extension of concrete crack development along the vertical branch of connectors and the concrete clove before metal material yielded. Also, Figs. 10(c)-(d) show a good agreement between the path of concrete crushing in the sample 6Da90-6 and finite element model. Failure modes predicted by finite element model are compared with those observed in push-out tests in Table 7. According to the table, in 83% of cases, failure modes predicted by finite element model are consistent with those observed in the test. The 17% error in prediction of failure modes can be due to concentration of shear load on one side of sample during the test that led to early failure of shear connector (see Fig. 10(e)).

### *4.5 Discussion*

In addition to verifying finite element model, push-out test on 12 DSCS samples shows that structures with complex interactions can be modeled with an acceptable speed and precision using explicit quasi-static analysis.

## 5. Conclusions

In this study, a 3D finite element model is presented using explicit quasi-static analysis based on push-out test on SCS samples with CSC connectors. In finite element model, only the welded connection of connectors to steel face plates was simplified and full connection is used based on the test, because failure was not observed in the welding area. The results of push-out tests showed that in spite of complexity of finite element model, load-slip behavior of CSC connectors and failure modes of SCS sandwich structures can be simulated with acceptable precision and speed using explicit quasi-static analysis. Using mass-scaling also reduced the analysis time significantly and prevented from non-convergence and early termination of finite element analysis.

## References

ABAQUS, S.M. and Manual, E.U.s. (2010), "Hibbitt", Karlsson & Sorensen Inc., Pawtucket, RI, USA.

Bowerman, H. and Chapman, J. (2000), "Bi-steel concrete steel sandwich construction", *Proceedings of the 4th US Engineering Foundation Conference on Composite Construction*, June.

Foundoukos, N. and Chapman, J. (2008), "Finite element analysis of steel–concrete–steel sandwich beams", *J. Constr. Steel Res.*, **64**(9), 947-961.

Huang, Z. and Liew, J. (2016), "Numerical studies of steel-concrete-steel sandwich walls with J-hook connectors subjected to axial loads", *Steel Compos. Struct., Int. J.*, **21**(3), 461-477.

Lee, J. and Fenves, G.L. (1998), "Plastic-damage model for cyclic loading of concrete structures", *J. Eng. Mech.*, **124**(8), 892-900.

Leekitwattana, M., Boyd, S. and Shenoi, R. (2010), "An alternative design of steel-concrete-steel sandwich beam", *Proceedings of the 9th International Conference on Sandwich Structures*.

Leekitwattana, M., Boyd, S. and Shenoi, R. (2011), "Evaluation of the transverse shear stiffness of a steel bi-directional corrugated-strip-core sandwich beam", *J. Constr. Steel Res.*, **67**(2), 248-254.

Liew, J.R. and Sohel, K. (2009), "Lightweight steel–concrete–steel sandwich system with J-hook connectors", *Eng. Struct.*, **31**(5), 1166-1178.

Liew, J.R., Sohel, K. and Koh, C. (2009), "Impact tests on steel–concrete–steel sandwich beams with lightweight concrete core", *Eng. Struct.*, **31**(9), 2045-2059.

Lubliner, J., Oliver, J., Oller, S. and Onate, E. (1989), "A plastic-damage model for concrete", *Int. J. Solids Struct.*, **25**(3), 299-326.

Shanmugam, N., Kumar, G. and Thevendran, V. (2002), "Finite element modelling of double skin composite slabs", *Finite Elem. Anal. Des.*, **38**(7), 579-599.

Shariati, M., Sulong, N.R., Suhatril, M., Shariati, A., Khanouki, M.A. and Sinaei, H. (2012), "Behaviour of C-shaped angle shear connectors under monotonic and fully reversed cyclic loading: an experimental study", *Mater. Des.*, **41**, 67-73.

Smitha, M. and Kumar, S.S. (2013), "Steel–concrete composite flange plate connections—finite element modeling and parametric studies", *J. Constr. Steel Res.*, **82**, 164-176.

Solomon, S., Smith, D. and Cusens, A. (1976), "Flexural tests of steel-concrete-steel sandwiches", *Mag. Concrete Res.*, **28**(94), 13-20.

Soty, R. and Shima, H. (2011), "Formulation for maximum shear force on L-shape shear connector subjected to strut compressive force at splitting crack occurrence in steel-concrete composite structures", *Procedia Engineering*, **14**, 2420-2428.

Tomlinson, M., Tomlinson, A., Li Chapman, M., Jefferson, A. and Wright, H. (1989), "Shell composite construction for shallow draft immersed tube tunnels", *Immersed Tunnel Techniques: Proceedings of the Conference*.

Valente, I. and Cruz, P.J. (2010), "Experimental analysis on steel and lightweight concrete composite beams", *Steel Compos. Struct., Int. J.*, **10**(2), 169-185.

Wright, H. and Oduyemi, T. (1991), "Partial interaction analysis of double skin composite beams", *J. Constr. Steel Res.*, **19**(4), 253-283.

Xie, M., Foundoukos, N. and Chapman, J. (2005), "Experimental and numerical investigation on the shear behaviour of friction-welded bar–plate connections embedded in concrete", *J. Constr. Steel Res.*, **61**(5), 625-649.

Yan, J.-B. (2015), "Finite element analysis on steel–concrete–steel sandwich beams", *Mater. Struct.*, **48**(6), 1645-1667.

Yan, J.-B., Liew, J.R., Zhang, M.-H. and Wang, J. (2014), "Ultimate strength behavior of steel-concrete-steel sandwich beams with ultra-lightweight cement composite, Part 1: Experimental and analytical Study", *Steel Compos. Struct., Int. J.*, **17**(6), 907-927.

Yan, J.-B., Liew, J. and Zhang, M.-H. (2015), "Ultimate strength behavior of steel-concrete-steel sandwich beams with ultra-lightweight cement composite, Part 2: Finite element analysis", *Steel Compos. Struct., Int. J.*, **18**(4), 1001-1021.

Yousefi, M. and Ghalehnovi, M. (2017), "Push-out test on the one end welded corrugated-strip connectors in steel-concrete-steel sandwich structure", *Steel Compos. Struct., Int. J.*, **24**(1), 23-35.

Zou, G.P., Xia, P.X., Shen, X.H. and Wang, P. (2016), "Investigation on the failure mechanism of steel-concrete steel composite beam", *Steel Compos. Struct., Int. J.*, **20**(6), 1183-1191.

*CC*